Stability Derivative Measurements with Magnetically Suspended Cone-Cylinder Models

D. Bharathan* and S.S. Fisher†
University of Virginia, Charlottesville, Va.

In a feasibility study, the stability derivatives C_{m_α}, $C_{m_{\dot\alpha}}+C_{m_q}$, C_{z_α}, and $C_{z_{\dot\alpha}}+C_{z_q}$ for 5- and 7-caliber cone-cylinder models are measured at $M=0.071$ and $Re=1.3\times10^4$ by suspending each model electromagnetically in a small subsonic wind tunnel, forcing it in periodic combined pitching and lateral motion at frequencies near pitch resonance, and comparing its frequency response with flow to that without flow. Drag coefficients are measured as well. The apparatus and techniques employed are described, the analytical model used to extract the derivatives from the response data is outlined, typical response data are shown, and comparisons are made with conventionally obtained similar data from other facilities.

Nomenclature‡

a	= axial distance between the model's center of mass and center of magnetization
$C_{m_\alpha}, C_{m_{\dot\alpha}}, C_{m_q}$	= aerodynamic pitching moment derivatives
C_x	= aerodynamic axial force coefficient
$C_{z_\alpha}, C_{z_{\dot\alpha}}, C_{z_q}$	= aerodynamic side-force derivatives
D	= differential operator
F	= lateral excitation force
f	= reduced excitation frequency
g	= gravitational acceleration
I_{x_0}	= steady-state vertical gradient-coil current
i_B	= model moment of inertia about a lateral axis through center of mass
k	= magnetic pitch stiffness
M	= Mach number
N_x	= core axial demagnetizing factor
n	= core shape factor, $(1-3N_x)/2(1-N_x)$
q	= model pitch velocity
Re	= model Reynolds number
s	= Laplace transform variable
w	= model lateral translational velocity
γ_x	= vertical coil force constant
ϵ_m	= magnetic damping moment coefficient
ϵ_z	= magnetic damping force coefficient
θ	= model pitch angle
μ	= model mass
ϕ	= transfer function phase angles

Introduction

PRELIMINARY stability evaluations for aerodynamic vehicles are usually carried out with sting-mounted models in wind tunnels or with models in free flight. In wind-tunnel tests, the influence of the sting can be significant. In free-flight tests observation time is usually severely limited and data retrieval is difficult. Magnetic suspension of wind-tunnel models eliminates the fluid-mechanics aspects of sting interference and allows testing over esentially unlimited time intervals. It has, however, generally been limited to small models and low dynamic pressures in applications to date.

The present investigation represents the initial application to stability testing of the electromagnetic suspension system employed here. These tests are aimed primarily at evaluating the practicality of measuring stability derivatives with this apparatus. They follow only a few stability investigations of somewhat limited scope conducted with magnetically suspended models elsewhere.[1-4] The original objective was to measure the pitching-moment derivative and the pitch-damping derivative for simple models. After the experiments were begun, it was found that side-force and side-damping derivatives could also be deduced.

Apparatus

The electromagnetic coil arrangement for the suspension system is shown in Fig. 1. A large pair of Helmholtz coils produces a uniform field to magnetize the model. A second pair of opposed coils create a streamwise (vertical) gradient in the field at the configuration centroid, the nominal model-support location. This gradient induces a force on the model which opposes its weight and drag. Third and fourth sets of coils create lateral (horizontal) gradients in the field which induce side forces on the model. All coils are water-cooled. The Helmholtz coils carry up to 200 A and produce a field of

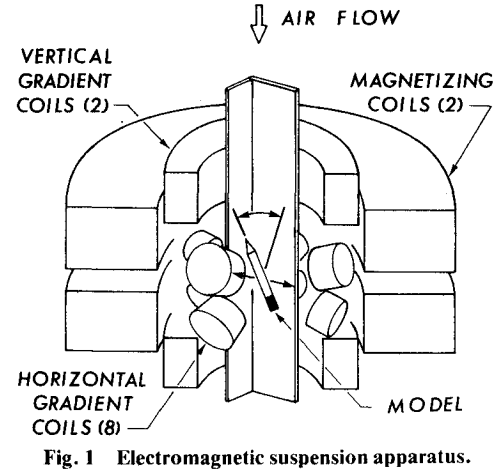

Fig. 1 Electromagnetic suspension apparatus.

Presented as Paper 77-79 at the AIAA 15th Aerospace Sciences Meeting, Los Angeles, Calif., Jan. 24-26, 1977; submitted Feb. 3, 1977; revision received Aug. 23, 1977.

Index categories: LV/M Testing, Flight and Ground; LV/M Dynamics and Control; Research Facilities and Instrumentation.

*Research Assistant; presently Research Associate, Thayer School of Engineering, Dartmouth College, Hanover, N.H. Member AIAA.

†Associate Professor, Mechanical and Aerospace Engineering. Member AIAA.

‡In this work, model velocity is normalized with the air speed, and electromagnetic lateral force is normalized with the flow dynamic pressure times model base area. For aerodynamic parameters, the model base diameter is used as the normalizing length.

up to 120,000 A/m at the model location. The vertical gradient coils carry up to 150 A and produce a field gradient as high as 390,000 A/m^2 at the model. The horizontal gradient coils carry up to 45 A and produce a gradient as high as 9,500 A/m^2 at the model.

The wind-tunnel test section is located inside the group of electromagnetic coils. This tunnel is a small, fan-driven, open-return tunnel with high contraction ratio. The test section is 11.4 cm by 11.4 cm by 30.0 cm long, the air speed for these tests was 24 m/s, and the flow turbulence level was 0.4%.

Model position is sensed optically using parallel light beams and silicon photocells. A feedback control system is used to keep the model centered near its nominal support location. For this, feedback signals indicative of the model's position along each of three orthogonal axes, after passing through appropriate compensating electronic networks, drive power amplifiers supplying current to respective sets of force coils.

For stability tests, the model is forced periodically in combined pitching and lateral motion. Model pitch orientation is monitored by sensing its lateral position at separate stations along its length. To reduce the effects of noise (due primarily to flow turbulence and secondarily to structural vibration and control-system noise), a digital signal averager is used and the several position-sensor and coil-current waveforms are averaged simultaneously by multiplexing the input to the averager.

The maximum dynamic pressure for these tests was fixed by the electromagnetic side force which could be applied on the model. At higher flow velocities, side forces due to flow turbulence and slight flow angularities exceeded the suspension system's capability to counteract them and thus resulted in loss of model support.

Other details concerning the apparatus and a more complete review of its development and operation are given in Ref. 5.

Models

The two models employed are simple cone cylinders. For each, the nose is a sharp 15.2 mm long cone with a 14.5 deg semivertex angle. The cylindrical afterbody, 7.8 mm in diameter, is 22.9 mm long for the 5-caliber model and 38.3 mm long for the 7-caliber model. The cylinder is hollow, with an inner diameter of 6.9 mm, and is machined from a single Lucite rod. The magnetic part of each model is a hollow steel (AISI-01) cylinder 6.9 mm o.d. by 6.3 mm i.d. by 12.7 mm long which fits tightly inside the aerodynamic shell. For each model, the downstream end of the shell and the core are coincident and the model base is carefully covered with plastic tape.

The models are made axisymmetric because model roll is uncontrolled in this suspension system, and position control and sensing would be prohibitively difficult for a rolling nonsymmetric model. The overall size of the model and core are limited by the wind tunnel's size (which in turn is limited by the space available between the coils) and the size of the region over which the magnetic field gradients are approximately constant. The relative sizing and mass of the aerodynamic shell and magnetic core, together with the imposed magnetic field, are chosen to place the model's pitch-resonance frequency above the bandwidth of the position-control system, to allow for a reasonably large aerodynamic drag, and to keep the electromagnetic damping small. This selection leaves the control system's effectiveness essentially unaltered while permitting adequate forced-motion amplitudes to be achieved near pitch resonance.

Procedure

For the tests, the model is driven magnetically with a sinusoidal lateral force at discrete frequencies in the vicinity of pitch resonance. Because the centers of mass of the model shell and core are not coincident, this excitation induces a combined pitching and lateral motion (predominantly pitching, since this motion is lightly damped). To simplify interpretation of the overall motion, the pitch-angle amplitude is always kept small, less than 0.5 deg. Thus, nonlinear aerodynamic and electromagnetic effects on the model motion are minimized and a number of cross-coupled electromagnetic forces and moments acting on the model are rendered negligible.

A theoretical model for the model's response is used to extract estimates for unknown aerodynamic and electromagnetic coefficients. This model provides analytical expressions for the model's transfer functions in pitch and in lateral translation. These expressions are algebraic functions of the aerodynamic and electromagnetic coefficients, and the unknown coefficients are determined by fitting the model frequency-response data to these expressions in a least-squares sense using a standard fitting code.[6]

Transfer-function amplitudes and phases are obtained by computer processing the recorded averaged position-sensor signal waveforms and coil-current waveforms. For this, measured position-sensor and force-current calibrations are used to convert raw data to positions, angles, velocities, and forces. This data processing yields plots vs frequency of 1) transfer-function amplitudes θ_0/F_0 and w_0/F_0, and 2) transfer-function phase angles ϕ_θ and ϕ_w, the angles by which the pitch orientation and the lateral velocity lead the perturbing force.

Transfer-function variations are measured both with flow and without flow. Simple flow-off (rather than vacuum) measurements are satisfactory because still-air damping is negligible compared to electromagnetic damping. From the flow-off data, the unknown electromagnetic force and moment coefficients are determined and, once these are known, the aerodynamic force and moment coefficients can be determined from the flow-on data.

Theoretical Transfer Functions

For slowly spinning models undergoing combined pitch and lateral motion, if magnetic damping in pitch and lateral translation are assumed linearly proportional to the pitching and lateral velocities, respectively (both are reasonable assumptions here), the governing equations of motion are[5]:

$$M_{11}w + M_{12}\theta = F \tag{1}$$

$$M_{21}w + M_{22}\theta = -aF \tag{2}$$

where

$$M_{11} = [2\mu - C_{z_{\dot\alpha}}] + [\epsilon_z - C_{z_\alpha}]$$

$$M_{12} = -[C_{z_{\dot\alpha}} + C_{z_q} + \epsilon_z a]D - [\gamma_x I_{x_0}(1+n) + C_{z_\alpha} - 2\mu g]$$

$$M_{21} = -[C_{m_{\dot\alpha}}D + C_{m_\alpha} + \epsilon_z a]$$

$$M_{22} = i_B D^2 + [\epsilon_m + \epsilon_z a^2 - C_{m_{\dot\alpha}} - C_{m_q}]D + [k + \gamma_x I_{x_0}(1+n)a - C_{m_\alpha}]$$

For the present tests where pitch and lateral velocity amplitudes are limited to 0.02 and 0.003, respectively, it can be shown[5] that M_{11} can be approximated by $2\mu D$. Also, in Eq. (2), the absolute value of $M_{21}w$ is less than 4% of $M_{22}\theta$ and can be neglected. Laplace transforms of Eqs. (1) and (2) then yield the following expressions for the steady-state model transfer functions:

$$\frac{W}{F} = \frac{F_1[s^2 + 2P_2P_3s + P_3^2]}{s[s^2 + 2P_5P_6s + P_6^2]} \tag{3}$$

$$\frac{\theta}{F} = \frac{P_4}{[s^2 + 2P_5P_6s + P_6^2]} \tag{4}$$

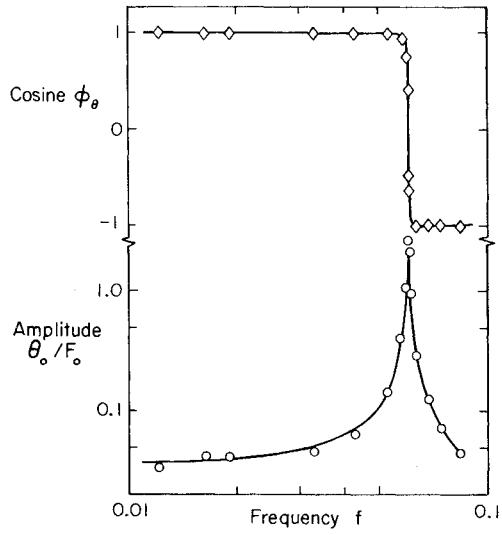

Fig. 2 Pitch transfer function, 5-caliber model, flow-off.

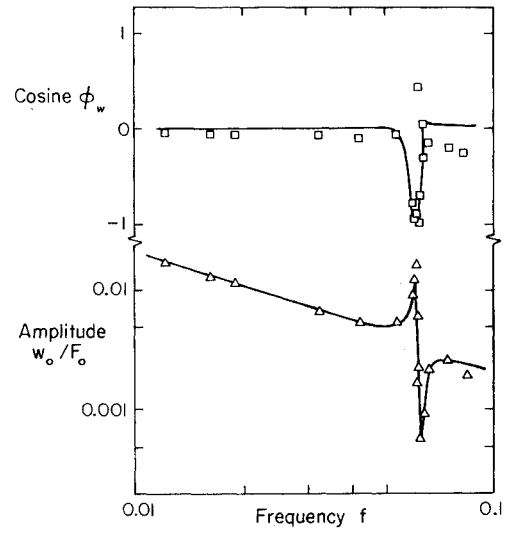

Fig. 3 Lateral velocity transfer function, 5-caliber model, flow-off.

where

$$P_1 = 1/2\mu$$

$$P_3^2 = [k+2\mu g a - C_{m_\alpha} - aC_{z_\alpha}]/i_B$$

$$2P_2P_3 = [\epsilon_m - a(C_{z_{\dot\alpha}} + C_{z_q}) - (C_{m_{\dot\alpha}} + C_{m_q})]/i_B$$

$$P_4 = -a/i_B$$

$$P_6^2 = [k+\gamma_x I_{x_0}(1+n)a - C_{m_\alpha}]/i_B$$

$$2P_5P_6 = [\epsilon_m + a^2\epsilon_z - (C_{m_{\dot\alpha}} + C_{m_q})]/i_B$$

Transfer Function Data

Measured flow-off variations for the pitch transfer function for the 5-caliber model are shown in Fig. 2. These data as well as those in the following figures are taken from four independent sets of measurements. Two sets (an original plus a repeat at a later date) were taken with excitation along one lateral axis; the other two were obtained with excitation rotated 90° horizontally. Within the data scatter, the four sets of data were identical. Thus, to plot the figures and preserve clarity, only a few representative data points are included. Also, in these figures, the phase data are presented as cos ϕ rather than ϕ itself.

The curve through the amplitude data in Fig. 2 is the least-squares-fitted version of Eq. (4). With the values of P_i ($i=1\rightarrow6$) determined by this match to the amplitude data, the curve shown thorugh the phase data is obtained. These two curves are merely those for resonance of a simple damped oscillator. The amplitude exhibits a sharp peak at the resonant frequency and across this peak the phase changes rapidly by 180 deg. The excellent agreement between the plotted curves and the data is convincing evidence that the pitching motion is adequately modeled.

Flow-off lateral velocity transfer-function data for this model are shown in Fig. 3. Again, the curve through the amplitude data is the least-squares fitted variation of Eq. (3) and the curve accompanying the phase data is that corresponding to the P_i values determined from the amplitude match. The sharp excursion in the amplitude data shows that, while the effect of lateral motion on pitch near resonance can be neglected, the reverse effect cannot. This excursion occurs because the net side force on the model is the sum of the imposed force F, and a second component, with both magnetic and gravitational contributions, induced by model pitch. Below resonance, θ and F are in phase, the two components add, and the lateral motion amplitude increases

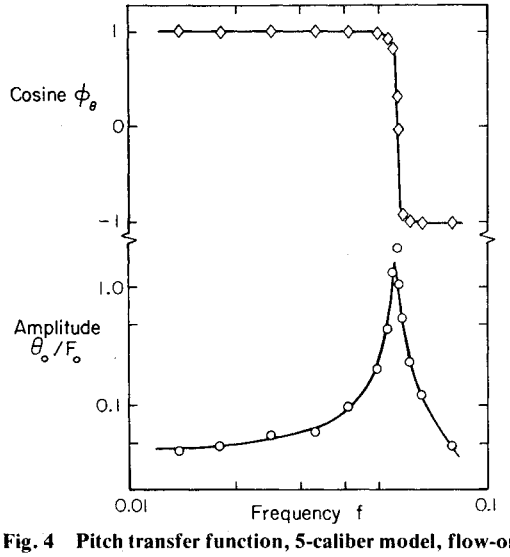

Fig. 4 Pitch transfer function, 5-caliber model, flow-on.

with increasing pitch amplitude. Above resonance, θ and F are out of phase and the result is the observed dip.

At frequencies well below resonance, as would be expected, cos ϕ_w approaches zero, corresponding to $\phi_w = -90$ deg. The dip in cos ϕ_w just below resonance is due to coupling between pitch and lateral motions. The measured overshoot in cos ϕ_w just above resonance is probably not real. It could easily be a result of inaccuracies in the phase measurement which become large whenever w_0 is small. The slight drop in the cos ϕ_w data below the predicted curve with increasing f also may not be real. Except near resonance, w_0/F_0 decreases roughly inversely with f, thus leading to increased inaccuracies in the ϕ_w measurement. Since P_i values are determined from matches to the more accurate amplitude data, these phase-measurement errors are relatively unimportant.

Corresponding flow-on response data for this model are shown in Figs. 4 and 5. Again, the curves through the amplitude data are fitted and the lines through the phase data correspond to the amplitude matches. The flow-on and the flow-off data are quite similar. With flow on, the pitch resonance frequency is reduced slightly due to the presence of the destabilizing aerodynamic pitching moment, and the width of the resonance peak is slightly increased due to aerodynamic damping. Also the excursion in the lateral velocity amplitude near pitch resonance is inverted, thus indicating that the aerodynamic side force (primarily due to

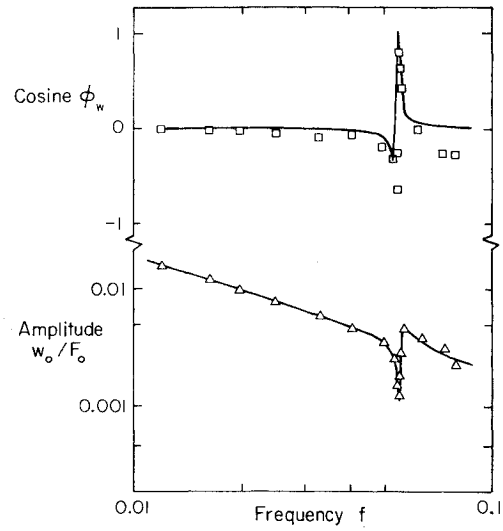

Fig. 5 Lateral velocity transfer function, 5-caliber model, flow-on.

C_{z_α}) is opposite in sign to and greater in magnitude than the sum of the magnetic and gravitational side forces. The noted disagreement between measured and predicted values of cos ϕ_w is again attributed to increased error in ϕ_w where w_0 is small.

Similar transfer function data and fits were also obtained for the 7-caliber model and these are given in Ref. 5.

Stabilitiy Derivatives

Deduced values of C_{z_α}, C_{m_α}, $C_{z_{\dot\alpha}}+C_{z_q}$, and $C_{m_{\dot\alpha}}+C_{m_q}$ are listed in Tables 1 and 2.[7-13] Values of the axial force (negative drag) coefficient C_x, also measured in these experiments, are listed as well. Analytical estimates and comparable measurements obtained elsewhere are also included. The analytical estimates are taken from the USAF DATCOM[7] (Data Compendium) and, except for C_x, are based on inviscid slender-body flow theory. No comparable data for $C_{z_{\dot\alpha}}+C_{z_q}$ for either model could be found in the literature, and comparable $C_{m_{\dot\alpha}}+C_{m_q}$ data could be found only for the 5-caliber model. Also, none of these other data are for exact matches of M, Re, or model shape. These parameters are reasonably close, however.

For the 5-caliber model, and C_{z_α} value, with 60% uncertainty (1σ), is 75% of the mean of other measurements and 20% below its analytical estimate; the large uncertainty for this measurement could readily explain either difference. The C_{m_α} value, with 3% uncertainty, is 3% above the mean of other measurements and 10% above its analytical estimate. The C_x value, with 2% uncertainty, compares well with its laminar analytical estimate, thus indicating a fully laminar boundary layer over this model. The $C_{m_{\dot\alpha}}+C_{m_q}$ measurement, with 50% uncertainty, is 10% below its analytical estimate and is at least of the same order of magnitude as the other measurements.§ The $C_{z_{\dot\alpha}}+C_{z_q}$ measurement, with essentially 100% uncertainty, is 30% of its analytical estimate and, as mentioned, no comparable experimental data could be found.

For the 7-caliber model, the measured C_{z_α} value, with 10% uncertainty, is 30% higher than its analytical estimate and 10% above the mean of the other measurements. The C_{m_α} value, with 3% uncertainty, is 15% below its analytical estimate and 10% below the mean of the other measurements. The C_x measurement, with 2% uncertainty, lies between the two analytical estimates, one assuming fully turbulent and the other fully laminar flow. This suggests a partially turbulent boundary layer over this longer model. The $C_{m_{\dot\alpha}}+C_{m_q}$ measurement, with 25% uncertainty, is 25% greater than its

§The axial stations of the moment-reference point for the $C_{m_{\dot\alpha}}+C_{m_q}$ data from Ref. 13 differ slightly from that for the present data. The $C_{z_{\dot\alpha}}$ and C_{z_q} data necessary to convert these data are not available. Despite this lack, the $C_{m_{\dot\alpha}}+C_{m_q}$ value for the 155-mm shell M101 compares reasonably well with the present result. The $C_{m_{\dot\alpha}}+C_{m_q}$ value for the 1/12th scale model, as suggested by the authors, is apparently in error.

Table 1 Data comparisons, 5-caliber model

Model[a]	A	B	C	D	E	F	F	G	H	I	Present tests
$Re_d \times 10^5$	4.4	5.0	5.0	6.4	5.3	2.2	2.4	2.1	1.8	0.13	0.13
M	0.15	0.2	0.2	0.26	0.5	0.2	0.4	0.6	0.7	0.07	0.07
C_{z_α} [b]	−1.98	−2.08	−2.42	−2.21	−1.8	−2.04	−2.04	−1.8	−1.8	−1.84	−1.5±0.9
C_{m_α}	4.19	1.75	2.05	3.7	4.31	4.91	4.51	4.09	4.01	3.28	3.6±0.1
C_x	...	...	...	...	...	...	...	−0.14	−0.13	−0.25[c] −0.21[d]	−0.21±0.005
$C_{m_{\dot\alpha}}+C_{m_q}$ [b]	...	...	...	...	...	...	...	−10.0[e]	4.6[f]	−3.63	−3.3±1.5
$C_{z_{\dot\alpha}}+C_{z_q}$	...	...	...	...	...	...	...	...	...	−8.27	−2.2±2.0

[a] A = 5-caliber Army-Navy spinner rocket with secant ogive nose (Ref. 8); B = 4.4-cal. with tangent ogive nose (Ref. 9); C = 5.9-cal. with tangent ogive nose (Ref. 9); D = 5-cal. with secand ogive nose (Ref. 10); E = 5.6-cal. with truncated conical nose, boat tail, and spiral grooves (Ref. 11); F = 3.8-cal 20-mm projectile with blunt conical nose, circumferential grooves, and projections (Ref. 12); G = 4.5-cal. 155-mm shell M101 with tangent ogive nose, boat tail, and spiral grooves (Ref. 13); H = 1/12 scaled model of G (Ref. 13); I = analytical estimate for 5-cal. model with conical nose (Ref. 7). [b] About a -point 3.4 calibers behind nose. [c] Assuming fully turbulent flow. [d] Assuming fully laminar flow. [e] About a point 3 calibers behind nose. [f] About a point 2.8 calibers behind nose.

Table 2 Data comparisons, 7-caliber model

Model[a]	A	B	C	D	E	F	Present tests
$Re_d \times 10^5$	4.3	7.3	7.3	5.0	6.4	0.13	0.13
M	0.15	0.25	0.25	0.2	0.26	0.07	0.07
C_{z_α} [b]	−1.81	−2.53	−2.48	−2.76	−2.18	−1.98	−2.6±0.3
C_{m_α}	6.58	6.17	7.42	6.97	5.87	6.97	5.9±0.15
C_x	...	...	..	...	...	−0.269[c]	−0.223±0.005
$C_{m_{\dot\alpha}}+C_{m_q}$ [b]	...	...	...	...	...	−11.6	−14.6±3.0
$C_{z_{\dot\alpha}}+C_{z_q}$	...	...	...	...	...	−13.7	−4.1±4.0

[a] A = 7-caliber Army-Navy spinner rocket with secant ogive nose (Ref. 8); B = 7-cal with conical nose (Ref. 8); C = 7-cal. with tangent ogive nose (Ref. 8); D = 7.1-cal. with tangent ogive nose (Ref. 9); E = 7-cal. with secant ogive nose (Ref. 10); F = analytical estimate for 7-cal. model with conical nose (Ref. 7). [b] About a point 4.6 calibers behind nose. [c] Assuming fully turbulent flow. [d] Assuming fully laminar flow.

analytical estimate. The $C_{z_{\dot{\alpha}}} + C_{z_q}$ value, with essentially 100% uncertainty, is 30% of its analytical estimate. As mentioned, no comparable data for $C_{m_{\dot{\alpha}}} + C_{m_q}$ or $C_{z_{\dot{\alpha}}} + C_{z_q}$ for this model were found.

The derivative estimates for the larger model are more precise than those for the smaller model. This occurs because the models had nearly identical magnetic forces and moments, while the aerodynamic forces were larger for the larger model.

Concluding Remarks

The present experiments demonstrate the feasibility of measuring selected stability derivatives in this facility. They also illustrate some of the complexities involved and some typical measurement uncertainty levels. For these models, they provide additional estimates for some of the aerodynamic derivatives and entirely new estimates for others. Since the main objective of these experiments was to measure pitching-moment and pitch-damping-moment derivatives, these derivatives are more accurately determined than their side-force counterparts.

A principal factor limiting measurement accuracy in these experiments was an experimental upper limit on wind-tunnel dynamic pressure, above which the model could not be maintained in stable support. The higher the dynamic pressure, however, the larger the differences between the model's flow-off and flow-on response, and thus the stability derivatives could be measured more precisely. Even with this limitation, the accuracy of the present data is comparable to that obtained by conventional means with considerably larger models and generally at higher flow dynamic pressures. Moreover, the present data are surely free of the fluid-mechanics aspects of sting interference. Also, with the excellent fits between the measured amplitudes and the modeling expressions, systematic errors in the derivative estimates are surely small.

With minor alteration of this technique, these experiments can be extended to higher flow speeds and to larger, finned, and probably rapidly spinning models. By using dummy stings, this approach could also be used to study sting interference.

Acknowledgment

Financial support for this research was provided by the Air Force Office of Scientific Research Grant 74-2705.

References

[1] Copeland, A.B., Covert, E.E., and Peterson, R.A., "Wind-Tunnel Measurement at $M=4.28$ of Some Static and Dynamic Aerodynamic Characteristics of Finned Missiles Suspended Magnetically," *Journal of Spacecraft and Rockets,* Vol. 5, July 1968, pp. 838-842.

[2] Vlajinac, M. and Gilliam, G.D., "Aerodynamic Testing of Conical Configurations Using a Magnetic Suspension System," MIT Aerospace Research Laboratories, Cambridge, Mass., Report ARL 70-0067, 1970.

[3] Goodyer, M.J., "Some Force and Moment Measurements Using Magnetically Suspended Models in a Low Speed Wind Tunnel," in *Summary of ARL Symposium on Magnetic Wind Tunnel Model Suspension and Balance Systems,* edited by F.L. Daum, Dayton University, Dayton, Ohio, July 1966, pp. 159-197.

[4] Judd, M., "The Magnetic Suspension System as a Wind Tunnel Dynamic Balance," *International Congress on Instrumentation in Aerospace Simulation Facilites Record,* IEEE, 1969, pp. 198-206.

[5] Bharathan, D., "Aerodynamic Stability Testing with Magnetically Suspended Models," Ph.D. Dissertation, University of Virginia, Charlottesville, Virginia, 1976; also, Air Force Office of Scientific Research Report AFOSR-TR-76-0036, 1976.

[6] Moore, R.H. and Ziegler,R.K., "The Solution of the General Least-Square Problem with Special Reference to High-Speed Computers," Los Alamos Scientific Laboratory, Los Alamos, New Mexico, Report LA 2367, Oct. 1959.

[7] Finck, R.D. and Hoak, D.E., "USAF Stability and Control DATCOM," Flight Control Division, Air Force Flight Dynamics Laboratory, Wright-Patterson Air Force Base, Dayton, Ohio, Oct. 1954.

[8] Greene, J.E., "Static Stability and Magnus Characteristics of the 5-caliber and 7-caliber Army-Navy Spinner Rocket at Low Subsonic Speeds," NAVORD Report 3884, Dec. 1954.

[9] Fletcher, C.A.J., "Investigation of the Magnus Characteristics of a Spinning Inclined Ogive-Cylinder Body at $M=0.2$," Australian Defense Scientific Service, TN HSA 159, Oct. 1969 (N70-35050).

[10] Nielson, G.I.T. and Platou, A.S., "The Effects of Conical Boat-Tails on the Magnus Characteristics of Projectiles at Subsonic and Transonic Speeds," Ballistic Research Laboratories, Report 1720, July 1974.

[11] Platou, A.S. and Nielson, G.I.T., "Some Aerodynamic Characteristics of the Artillery Projectile XM549," Ballistic Research Laboratories, Memorandum Report 2284, April 1974.

[12] Sieron, T.R., "The Magnus Characteristics of the 20 mm and 30 mm Projectiles in the Transonic Speed Range," Wright Air Development Center, TN 59-320, Oct. 1959.

[13] Karpov, B.G. and Schmidt, L.E., "The Aerodynamic Properties of the 155 mm Shell M-101 from Free-Flight-Range Tests of Full Scale and 1/12 Scale Models," Ballistic Research Laboratories, Memorandum Report 1582, June 1964.